Deep–Sea Research I 217 (2025) 104452

Contents lists available at ScienceDirect

Deep-Sea Research Part I

journal homepage: www.elsevier.com/locate/dsri

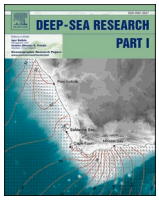

Interaction between the M_2 internal tides and typhoon-induced near-inertial waves near the Luzon Strait

Anzhou Cao [a,*], Zheng Guo [b], Xu Chen [c], Xinyu Guo [d], Jinbao Song [a]

[a] Ocean College, Zhejiang University, Zhoushan, China
[b] Marine Science and Technology College, Zhejiang Ocean University, Zhoushan, China
[c] Key Laboratory of Physical Oceanography, Ocean University of China, Qingdao, China
[d] Center for Marine Environmental Studies, Ehime University, Matsuyama, Japan

ARTICLE INFO

Keywords:
Internal tides
Near-inertial waves
interaction
Luzon Strait
Numerical simulation

ABSTRACT

The South China Sea is abundant with intense internal tides (ITs) and typhoon-induced near-inertial waves (NIWs), which inevitably interact with each other. Based on the numerical simulation results, the interaction between the M_2 ITs and typhoon Megi-induced NIWs in the deep ocean near the Luzon Strait is studied. The interaction gives rise to sum- and difference-frequency waves, denoted as the fM_2 and M_2-f waves. Results of this study highlight the contribution of the M_2-f waves to shear enhancement: The kinetic energy of the M_2-f waves is one order of magnitude smaller than that of the M_2 ITs, but the domain-averaged vertical shear squared caused by the M_2-f waves is comparable to that of the M_2 ITs. The IT-NIW interaction is dominated by the product of vertical internal tidal velocity and vertical shear of horizontal near-inertial velocity, which is followed by the product of horizontal near-inertial velocity and horizontal shear of horizontal internal tidal velocity. The IT-NIW interaction influences the evolution of near-inertial kinetic energy through modulating the energy exchange and near-inertial energy flux, which are site-dependent. In the modulation of energy exchange, the terms associated with horizontal shear of horizontal internal tidal velocity play crucial roles. Whereas in the modulation of near-inertial energy flux, the terms associated with vertical shear of horizontal near-inertial velocity are dominant.

1. Introduction

Internal tides (ITs) and near-inertial waves (NIWs) are typical internal waves, which are ubiquitous in the global ocean. Because ITs are generated by barotropic tidal currents flowing over varying topographies in the stratified ocean, intense ITs are usually found near rough topographies, such as the Luzon Strait (LS) and Hawaiian Ridge (Simmons et al., 2004; Niwa and Hibiya, 2011, 2014; Müller, 2013; Buijsman et al., 2016; Zhao, 2019). Unlike ITs, there are several different mechanisms that can generate NIWs, including wind, wave-wave interaction, Lee wave and spontaneous generation, among which wind is the most important (Alford et al., 2016). Both ITs and NIWs play crucial roles in enhancing the turbulent mixing in the ocean (e.g. Yang et al., 2016; Qiao et al., 2022). According to previous estimations (Munk and Wunsch, 1998; Carter et al., 2012), a total of 2 TW energy is required to maintain the abyssal ocean stratification with globally averaged diapycnal diffusivity of 10^{-4} m^2/s, in which both ITs and wind-induced NIWs contribute approximately 1 TW. Hence, investigating ITs and NIWs is of great importance to understand the ocean energy cascade.

As the largest marginal sea in the Northwest Pacific Ocean, the South China Sea (SCS) is famous for the intense ITs therein. Observations show that the westward IT energy flux radiated from the LS into the SCS could reach 40 ± 8 kW/m and this value exceeds any other known IT generation site around the world (Alford et al., 2015). At the LS which is the major generation site of ITs in the SCS, the peak-to-peak baroclinic velocity and vertical displacements often exceed 2 m/s and 300 m, respectively (Alford et al., 2011). The SCS is also abundant with intense NIWs, due to the active typhoons and monsoons. According to Wang et al. (2007), 10.3 typhoons pass over the SCS per year on average, which cause significant NIWs (e.g. Chen et al., 2013; Guan et al., 2014; Yang et al., 2015; Cao et al., 2018; Lin et al., 2022; He et al., 2022). The typhoons and monsoons also cause seasonal variability of near-inertial kinetic energy (NIKE) in the SCS, resulting in high NIKE in November–January and low NIKE in April–June (Li et al., 2022). The intense ITs and NIWs in the SCS inevitably interact with each other, which

* Corresponding author.
E-mail address: caoanzhou@zju.edu.cn (A. Cao).

https://doi.org/10.1016/j.dsr.2025.104452
Received 21 April 2024; Received in revised form 13 December 2024; Accepted 20 January 2025
Available online 28 January 2025

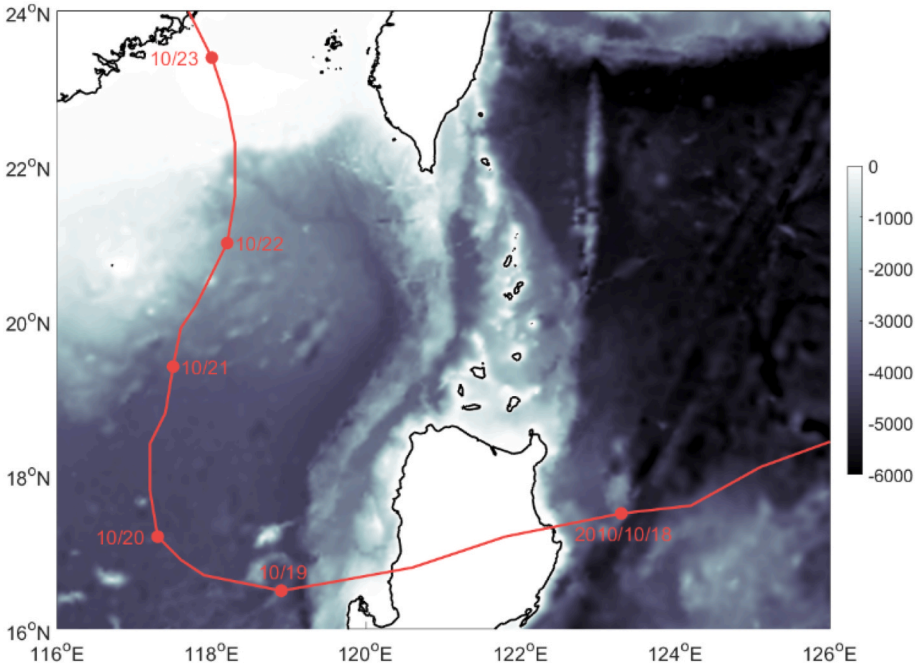

Fig. 1. Bathymetry (shading, unit: m) near the LS and typhoon Megi's track (the red curve). Time is labeled every one day. (For interpretation of the references to color in this figure legend, the reader is referred to the Web version of this article.)

generate internal waves with higher vertical wavenumber and make a considerable contribution to the shear enhancement in the ocean (Xing and Davies, 2002; Davies and Xing, 2003; Lin et al., 2015; Cao et al., 2018; Liu et al., 2018; Liang et al., 2019).

Previous studies have demonstrated that on the continental slope and shelf of the SCS, the product of vertical velocity of ITs and vertical shear of NIWs dominates over the product of vertical velocity of NIWs and vertical shear of ITs in the IT-NIW interaction (Xing and Davies, 2002; Davies and Xing, 2003; Guan et al., 2014; Lin et al., 2015; Liu et al., 2018). However, it is unclear whether this is also valid in the deep ocean. At the same time, contributions of other terms to the IT-NIW interaction have not been evaluated. Moreover, previous studies mainly focus on the sum-frequency waves generated by the IT-NIW interaction, of which the frequency is equal to the sum of IT frequency and NIW frequency. However, the difference-frequency waves, of which the frequency is equal to the difference of IT frequency and NIW frequency, are rarely studied. Furthermore, to what extent the IT-NIW interaction influences the evolution of NIKE remain unknown. These questions motivate the present study.

Based on the numerical simulation results, this study investigates the interaction between the M_2 ITs and NIWs induced by typhoon Megi (2010) in the deep ocean near the LS. The paper is organized as follows. The theory of IT-NIW interaction is introduced in section 2. The data and methods used in this study are introduced in section 3. The main results are presented in section 4. Section 5 contains discussions and conclusions.

2. Theory

The governing equation of the motion in the ocean can be written as

$$\frac{\partial \mathbf{u}}{\partial t} + \mathbf{u}\cdot\nabla\mathbf{u} = \mathrm{RHS}, \tag{1}$$

in which $\mathbf{u}=(u, v, w)$ is the velocity, t is the time, and RHS represents the right-hand-side terms including the Coriolis force, pressure gradient, gravity and turbulent viscosity. Assume that there only exist the M_2 ITs and NIWs in the motion system, and the velocity can be decomposed into two components:

$$\mathbf{u} = \mathbf{u}_T + \mathbf{u}_f, \tag{2}$$

in which subscripts $_T$ and $_f$ denote the M_2 ITs and NIWs, respectively. Following Hazewinkel and Winters (2011), Onuki and Hibiya (2015) and Wang et al. (2021), we can get the governing equation for the near-inertial velocity $\mathbf{u}_f$ after substituting Equation (2) into Equation (1) and making some simplifications:

$$\frac{\partial \mathbf{u}_f}{\partial t} + \mathbf{u}_f\cdot\nabla\mathbf{u}_T + \mathbf{u}_T\cdot\nabla\mathbf{u}_f = \mathrm{RHS}. \tag{3}$$

Because both ITs and NIWs are periodic motions, they can be rewritten as

$$\mathbf{u}_f = G(ft) \text{ and } \mathbf{u}_T = G(\omega t), \tag{4}$$

in which G represents the sinusoidal or cosinusoidal function, f is the Coriolis frequency, and ω is the frequency of the M_2 ITs. Combining Equations (3) and (4), it is easy to know that both $\mathbf{u}_f\cdot\nabla\mathbf{u}_T$ and $\mathbf{u}_T\cdot\nabla\mathbf{u}_f$ can cause $G[(\omega+f)t]$ and $G[(\omega - f)t]$, i.e. the periodic motions with frequencies of ω+f and ω-f, corresponding to the fM$_2$ and M$_2$-f waves.

Multiplying Equation (3) by $\mathbf{u}_f$, we can get the equation for NIKE (E_f):

$$\frac{\partial E_f}{\partial t} + \mathbf{u}_f\cdot(\mathbf{u}_f\cdot\nabla)\mathbf{u}_T + \mathbf{u}_f\cdot(\mathbf{u}_T\cdot\nabla)\mathbf{u}_f = \mathrm{RHS}. \tag{5}$$

Note that the water density is not considered in the NIKE in Equation (5). According to Hazewinkel and Winters (2011), Onuki and Hibiya (2015) and Wang et al. (2021), $\mathbf{u}_f\cdot(\mathbf{u}_f\cdot\nabla)\mathbf{u}_T$ denotes the energy exchange between ITs and NIWs, and $\mathbf{u}_f\cdot(\mathbf{u}_T\cdot\nabla)\mathbf{u}_f$ modulates the divergence of near-inertial energy flux. Hence, the IT-NIW interaction can influence the evolution of NIKE through modulating the energy exchange and near-inertial energy flux, as Equation (5) can be changed to

$$\frac{\partial E_f}{\partial t} = -\mathbf{u}_f\cdot(\mathbf{u}_f\cdot\nabla)\mathbf{u}_T - \mathbf{u}_f\cdot(\mathbf{u}_T\cdot\nabla)\mathbf{u}_f + \mathrm{OTH}, \tag{6}$$

where OTH denotes the RHS terms in Equation (5).

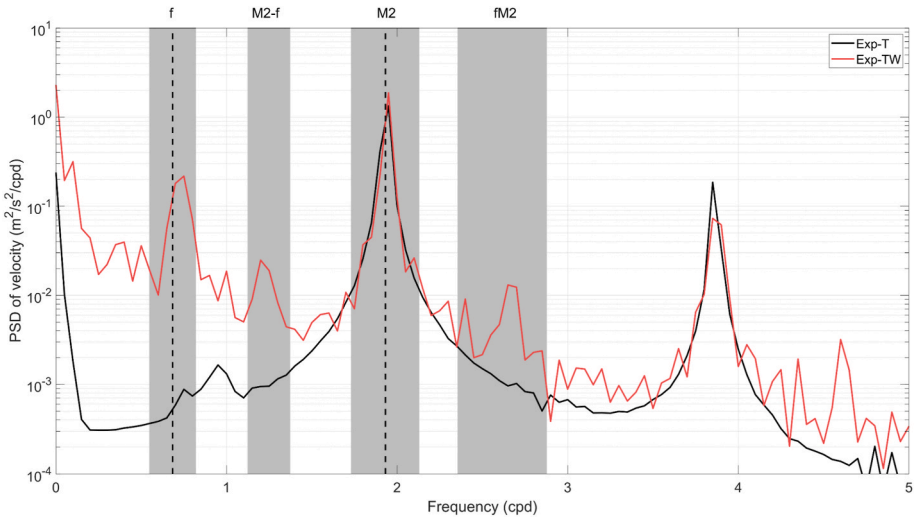

Fig. 2. Depth-averaged power spectral densities (PSDs) of zonal baroclinic velocity at 120°E, 20°N in Exp-T (the black curve) and Exp-TW (the red curve). The vertical dashed lines indicate the local Coriolis frequency and the M_2 tidal frequency. The shadings denote the cutoff frequencies for NIWs, M_2 ITs, fM_2 and M_2-f waves. (For interpretation of the references to color in this figure legend, the reader is referred to the Web version of this article.)

3. Data and methods

3.1. Data

In this study, the numerical simulation results (Exp-TW) of Cao et al. (2023a) are used to investigate the interaction between the M_2 ITs and typhoon-induced NIWs in the deep ocean near the LS. In this experiment, only the M_2 tidal forcing and wind forcing are considered to drive the Coastal and Regional Ocean COmmunity model (CROCO) to simultaneously simulate the M_2 ITs and wind-driven NIWs near the LS. The simulation domain ranges from 115.5°E to 126.5°E and from 15.5°N to 24.5°N with the LS located at the center (Fig. 1). The domain includes four 0.5° sponge layers at the open boundaries. The horizontal resolution of the model is 1/20° and there are 30 uneven sigma layers in the vertical direction. In this experiment, the real wind forcing (hourly Climate Forecast System Reanalysis wind data downloaded from apdrc.soest.hawaii.edu/data/data.php) in October 2010 is used, which includes the passage of typhoon Megi (Fig. 1). The M_2 tidal forcing is obtained from the Oregon State University global models of ocean tides (TPXO7; Egbert and Erofeeva, 2002). The initial stratification is horizontally homogeneous, which is obtained from the horizontally averaged temperature and salinity of the HYbrid Coordinate Ocean Model reanalysis data (apdrc.soest.hawaii.edu/data/data.php) in the domain on October 1, 2010. The experiment is run from October 1 to 31, 2010

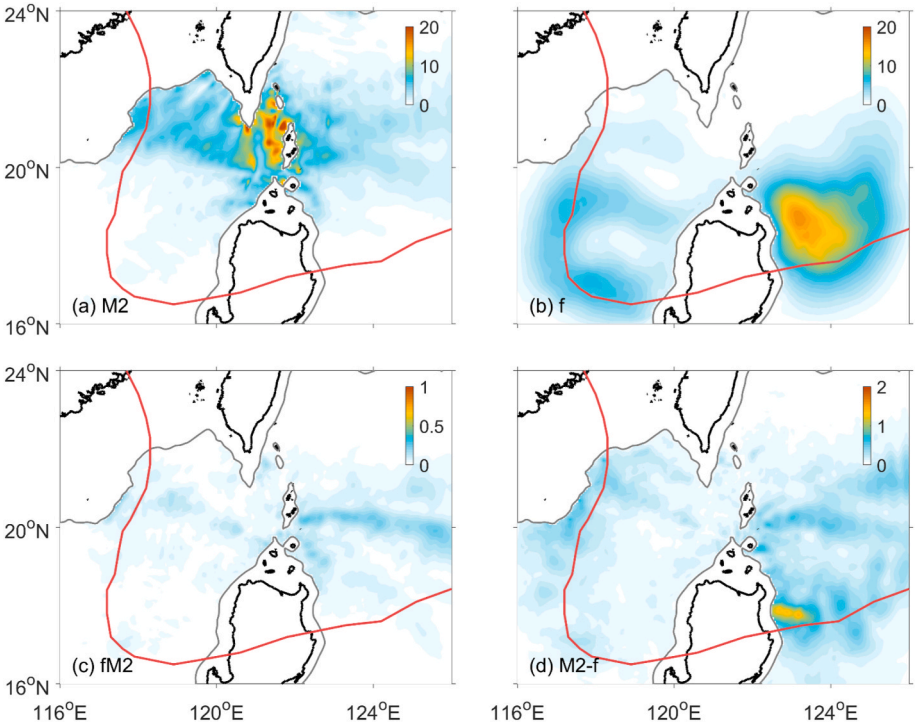

Fig. 3. Time-averaged depth-integrated KE (shading, unit: kJ/m^2) of (a) the M_2 ITs, (b) NIWs, (c) fM_2 and (d) M_2-f waves. The red curve denotes typhoon Megi's track and the gray curve denotes the 1000 m isobath. Note that the colorbar varies with subfigure. (For interpretation of the references to color in this figure legend, the reader is referred to the Web version of this article.)

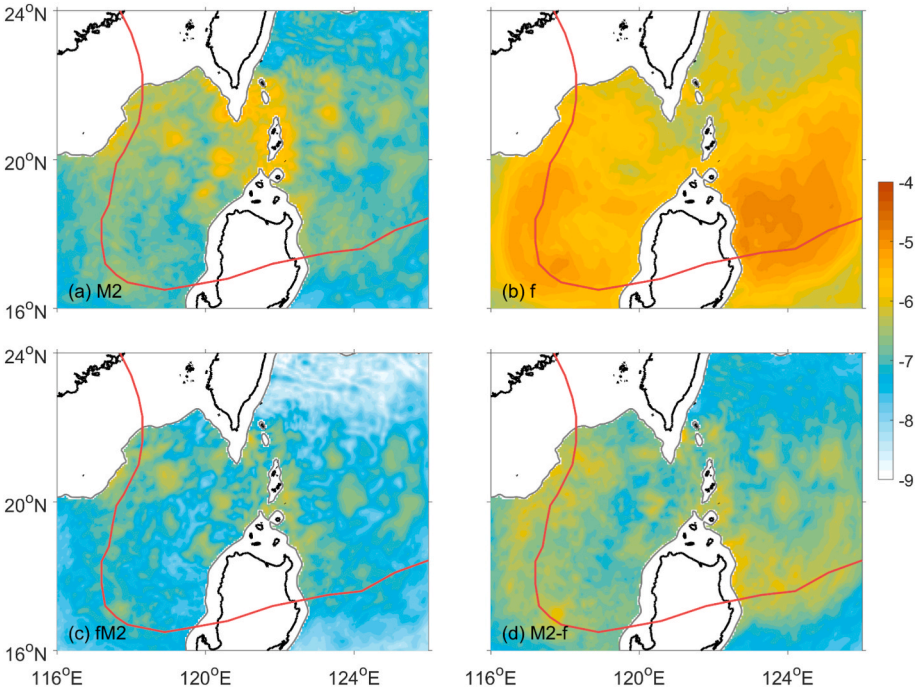

Fig. 4. Time-averaged vertical shear squared (shading, unit: s^{-2}, in the log form) of (a) the M_2 ITs, (b) NIWs, (c) fM_2 and (d) M_2-f waves averaged in the upper 1000 m. The red curve denotes typhoon Megi's track and the gray curve denotes the 1000 m isobath. (For interpretation of the references to color in this figure legend, the reader is referred to the Web version of this article.)

and the simulation results are output every 1 h. Moreover, the simulation results of Exp-T of Cao et al. (2023a), in which only the M_2 tidal forcing is considered, are used as a comparison. Refer to Cao et al. (2023a) for more details about these experiments.

3.2. Methods

Because the main aim of this study is to investigate the internal waves generated by the interaction between the M_2 ITs and NIWs, the forth-order Butterworth bandpass filter is employed to extract these internal waves. Before filtering, spectral analysis is conducted to determine the cutoff frequencies for NIWs, M_2 ITs, fM_2 and M_2-f waves (Fig. 2). According to the spectral analysis results, the cutoff frequencies for NIWs, fM_2 and M_2-f waves are set to [0.80, 1.20]f, [0.90, 1.10]fM_2 and [0.90, 1.10]M_2-f, respectively, and the cutoff frequency for the M_2 ITs is [1.73, 2.13] cpd (Zhao et al., 2010; Guo et al., 2012; Cao et al., 2017). These cutoff frequencies are sufficiently wide to extract the corresponding internal waves and narrow enough to separate them from other internal waves (Fig. 2). Considering the time of typhoon Megi entering and leaving the study domain as well as the boundary effect of filtering, the results from October 15 to 24 (a total of 10 days) are used for the following analysis. Thereafter, the kinetic energy (KE) and vertical shear squared of the M_2 ITs, NIWs, fM_2 and M_2-f waves are calculated as:

$$\mathrm{KE} = \frac{1}{2}\rho\left(\widetilde{u}^2 + \widetilde{v}^2\right), \tag{7}$$

$$s^2 = \left(\frac{\partial \widetilde{u}}{\partial z}\right)^2 + \left(\frac{\partial \widetilde{v}}{\partial z}\right)^2, \tag{8}$$

where $\widetilde{u}$ and $\widetilde{v}$ denote the zonal and meridional velocities of the M_2 ITs, NIWs, fM_2 or M_2-f waves, ρ is the water density and z is the coordinate of vertical direction. All the terms in $\mathbf{u}_f\cdot\nabla\mathbf{u}_T + \mathbf{u}_T\cdot\nabla\mathbf{u}_f$ are computed to evaluate their contributions to the IT-NIW interaction. We also calculate $-\mathbf{u}_f\cdot(\mathbf{u}_f\cdot\nabla)\mathbf{u}_T$ and $-\mathbf{u}_f\cdot(\mathbf{u}_T\cdot\nabla)\mathbf{u}_f$ to explore the influence of IT-NIW interaction on the evolution of NIKE. Because this study mainly focuses on the IT-NIW interaction in the deep ocean, we only show and discuss the results where the local water depth exceeds 1000 m.

4. Results

4.1. KE

Fig. 3 displays the time-averaged depth-integrated KE of the M_2 ITs, NIWs, fM_2 and M_2-f waves during the passage of typhoon Megi. It is clearly shown that large M_2 KE is mainly concentrated at the LS (Fig. 3a), as it is the major generation site of ITs in the SCS. The M_2 KE is gradually damped along the eastward- and westward-propagating beams (Miao et al., 2011), but rapidly damped along the southwestward-propagating beam. This is consistent with the observed and simulated M_2 baroclinic energy flux near the LS (e.g. Zhao, 2014; Guo et al., 2020). Large NIKE mainly appears along typhoon Megi's track (Fig. 3b). Moreover, due to the blocking of the Luzon Island, the NIKE is accumulated to the east of the Luzon Island and reaches the peak value which is twice as large as that in the SCS. The fM_2 and M_2-f KE is concentrated near both the LS and Megi's track (Fig. 3c and d). The peak values of the fM_2 and M_2-f KE are one order of magnitude smaller than those of the M_2 KE and NIKE, which is consistent with the spectral analysis result (Fig. 2a) and previous observations (Lin et al., 2015; Liu et al., 2018). It is worthy to note that the M_2-f waves have larger KE than the fM_2 waves, with the domain-averaged M_2-f KE almost 4 times larger than the domain-averaged fM_2 KE. This result highlights the importance of the M_2-f waves in the interaction between the M_2 ITs and NIWs. In addition, for the NIWs, fM_2 and M_2-f waves, the KE in the upper 1000 m accounts for more than 90% of the depth-integrated KE. Therefore, we mainly focus on the results in the upper 1000 m in the followings.

4.2. Vertical shear

Attention is then paid to the vertical shear caused by the M_2 ITs, NIWs, fM_2 and M_2-f waves. Because a sigma coordinate is adopted in the vertical direction in the CROCO, the extracted velocities of the M_2 ITs,

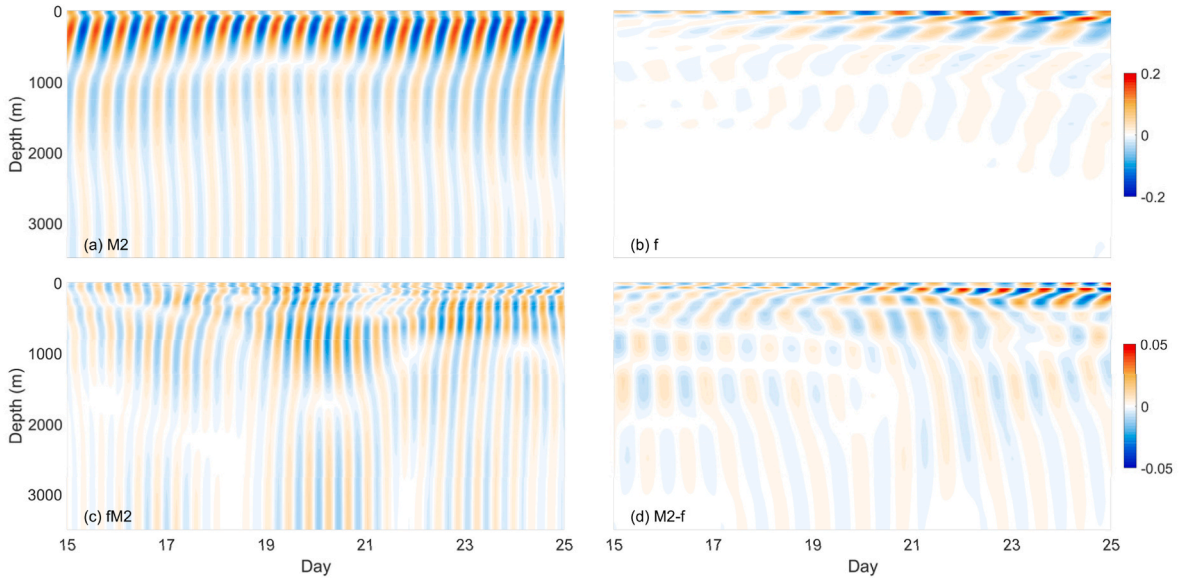

Fig. 5. Zonal velocities (shading, unit: m/s) of (a) the M_2 ITs, (b) NIWs, (c) fM_2 and (d) M_2-f waves at 120°E, 20°N. Note that the colorbar varies for the upper and lower panels.

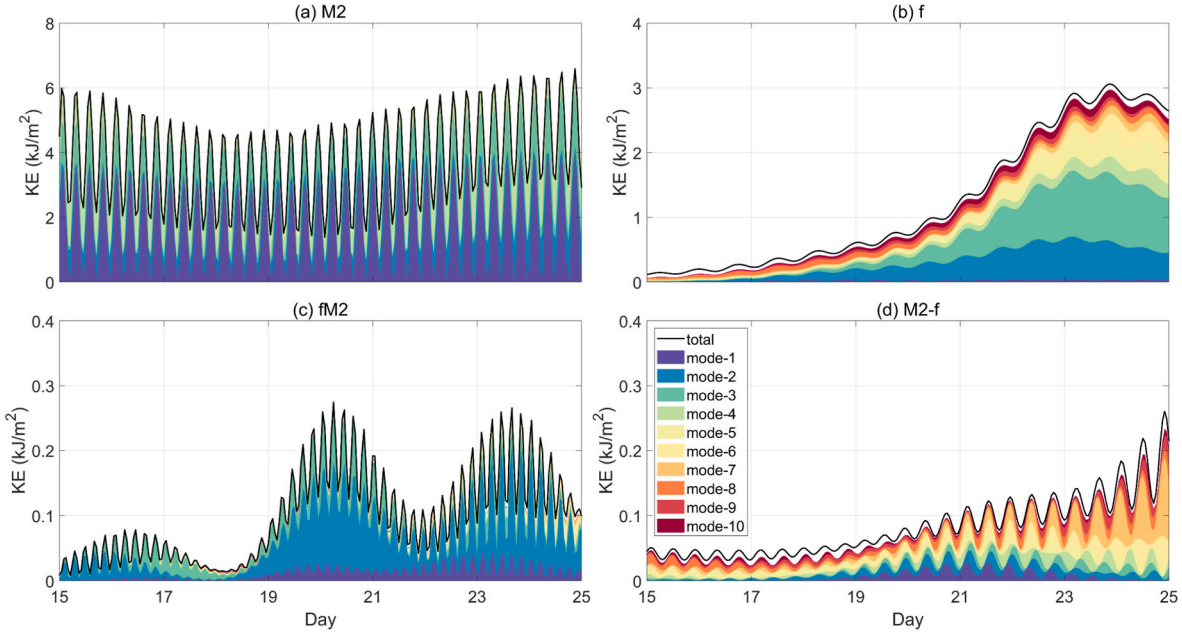

Fig. 6. Depth-integrated KE (black curve) and its modal content (colored shadings) of (a) the M_2 ITs, (b) NIWs, (c) fM_2 and (d) M_2-f waves at 120°E, 20°N.

NIWs, fM_2 and M_2-f waves are first linearly interpolated onto 5 m uniform vertical layers before the calculation of vertical shear squared (Equation (8)). Fig. 4 shows the time-averaged shear squared of the M_2 ITs, NIWs, fM_2 and M_2-f waves averaged in the upper 1000 m, as the shear squared in each band below 1000 m depth is at least one order of magnitude smaller than that in the upper 1000 m. From the perspective of spatial distribution, the shear squared in each band almost shares a similar pattern as the corresponding KE (Fig. 3). Large M_2 and near-inertial shear squared mainly appears at the LS and along typhoon Megi's track, respectively, consistent with the fact that high-mode ITs and NIWs usually dissipate locally and cannot propagate a long distance away from the generation site (St. Laurent et al., 2002; Alford, 2020). The fM_2 and M_2-f waves, as the resulting waves of the interaction between the M_2 ITs and NIWs, cause significant shear both at the LS and along Megi's track. In terms of intensity, the near-inertial shear squared is one order of magnitude larger than the M_2 shear squared, for both peak (1.47×10^{-5} s^{-2} for NIWs and 5.87×10^{-6} s^{-2} for the M_2 ITs) and domain-averaged values (2.82×10^{-6} s^{-2} for NIWs and 2.36×10^{-7} s^{-2} for the M_2 ITs). This result is consistent with observations in the SCS during typhoon periods (Cao et al., 2019). The shear squared caused by the M_2-f waves is stronger than that caused by the fM_2 waves for both peak (1.00×10^{-6} s^{-2} for the fM_2 waves and 1.52×10^{-6} s^{-2} for the M_2-f waves) and domain-averaged values (6.68×10^{-8} s^{-2} for the fM_2 waves and 2.04×10^{-7} s^{-2} for the M_2-f waves). Moreover, it is interesting to find that the domain-averaged shear squared caused by the M_2-f waves is comparable to that caused by the M_2 ITs. Considering that the M_2-f KE (Fig. 3d) is one order of magnitude smaller than the M_2 KE (Fig. 3a), this result highlights the contribution of the M_2-f waves to shear enhancement.

The stronger vertical shear caused by the NIWs (M_2-f waves)

Table 1
Proportions (%) of modal KE in the total KE for the M_2 ITs, NIWs, fM_2 and M_2-f waves at 120°E, 20°N.

Mode	1	2	3	4	5	6	7	8	9	10
M_2 ITs	47.9	12.1	17.7	19.6	1.8	<1.0	<1.0	<1.0	<1.0	<1.0
NIWs	2.0	22.5	29.7	6.9	11.3	5.3	3.4	5.3	3.6	4.6
fM_2 waves	12.3	53.5	20.5	3.1	4.0	<1.0	<1.0	<1.0	<1.0	<1.0
M_2-f waves	7.6	9.6	6.0	8.8	9.2	10.2	17.7	9.9	7.6	3.3

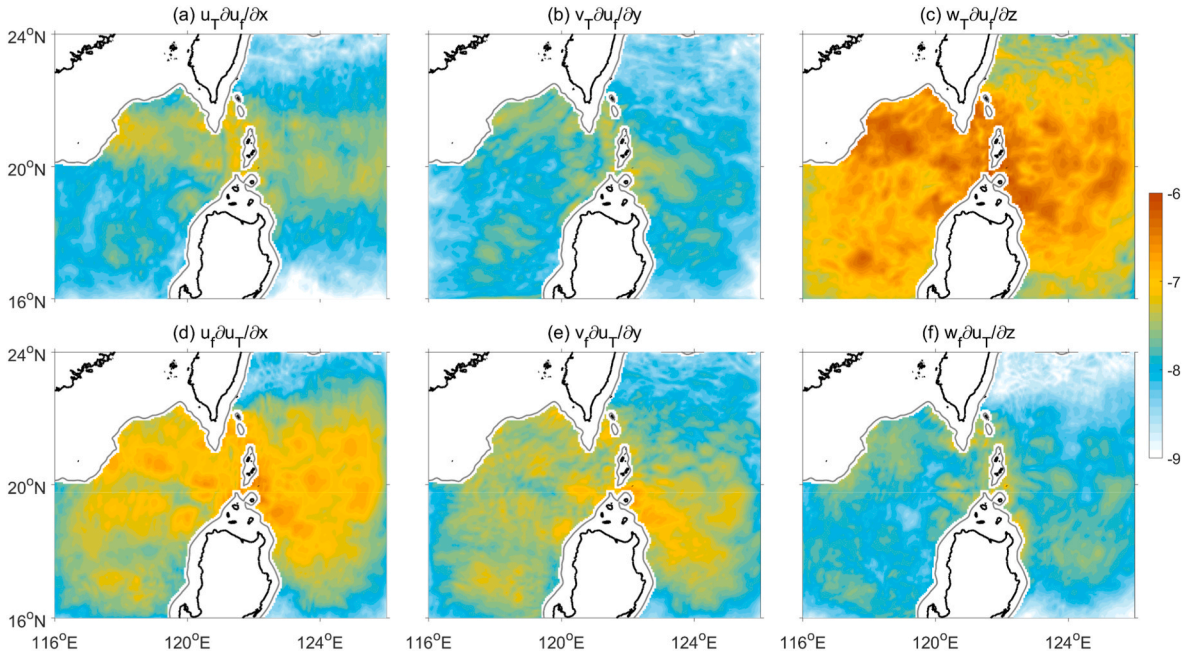

Fig. 7. Time-averaged magnitude (shading, unit: m/s^2, in the log form) of (a) $u_T\partial u_f/\partial x$, (b) $v_T\partial u_f/\partial y$, (c) $w_T\partial u_f/\partial z$, (d) $u_f\partial u_T/\partial x$, (e) $v_f\partial u_T/\partial y$, and (f) $w_f\partial u_T/\partial z$ averaged in the upper 1000 m. The gray curve denotes the 1000 m isobath.

compared to the M_2 ITs (fM_2 waves) is attributed to their more complex vertical structure. As displayed in Fig. 5, the M_2 ITs and fM_2 waves show apparent dominance of low modes (mode-1 and mode-2), whereas the NIWs and M_2-f waves exhibit signature of high modes (higher than mode-3). To further demonstrate this, modal decomposition (e.g. Zhao et al., 2010;Cao et al., 2023b) is conducted for the M_2 ITs, NIWs, fM_2 and M_2-f waves at 120°E, 20°N, and corresponding results are displayed in Fig. 6 and Table 1. It is clearly shown that mode-1 dominates the M_2 ITs, which accounts for 47.9% of the total M_2 KE, and mode-2 dominates the fM_2 waves, which accounts for 53.5% of the total fM_2 KE. In contrast, the NIWs are dominated by mode-3 and M_2-f waves are dominated by mode-7. Moreover, for both the M_2 ITs and fM_2 waves, their KE is mainly concentrated in the first five modes, the sum of which accounts for more than 90% of the total KE, and mode-6 to mode-10 are negligible. In contrast, mode-6 to mode-10 play non-negligible roles in the NIWs and M_2-f waves, contributing 22.2% of the total NIKE and 48.7% of the total M_2-f KE. These results indicate that the differences in modal content lead to variations in the vertical structure and hence shear intensity among the M_2 ITs, NIWs, fM_2 and M_2-f waves.

4.3. Contribution of each term in the IT-NIW interaction

In the interaction between the M_2 ITs and NIWs, the advection term $\mathbf{u}_f\cdot\nabla\mathbf{u}_T+\mathbf{u}_T\cdot\nabla\mathbf{u}_f$ in the momentum equation generates the fM_2 and M_2-f waves (Equation (3)). For each component of velocity (u, v and w), the advection term can be divided into six terms. In the following, we will show the magnitude of these six terms for zonal velocity u as an example. Similar results are found for the other velocity components. The six terms for zonal velocity u are $u_T\partial u_f/\partial x$, $v_T\partial u_f/\partial y$, $w_T\partial u_f/\partial z$, $u_f\partial u_T/\partial x$, $v_f\partial u_T/\partial y$, and $w_f\partial u_T/\partial z$, of which the time-depth-averaged magnitude is shown in Fig. 7. It is easy to find that in the interaction between the M_2 ITs and NIWs, the product of vertical internal tidal velocity and vertical shear of horizontal near-inertial velocity ($w_T\partial u_f/\partial z$; Fig. 7c) dominates over the other five terms, and the product of vertical near-inertial velocity and vertical shear of horizontal internal tidal velocity ($w_f\partial u_T/\partial z$; Fig. 7f) is the weakest among the six terms. On the average, $w_T\partial u_f/\partial z$ is 1–2 orders of magnitude larger than $w_f\partial u_T/\partial z$. This is consistent with previous observations and simulations on the continental slope and shelf of the SCS (Xing and Davies, 2002; Davies and Xing, 2003; Guan et al., 2014; Lin et al., 2015; Liu et al., 2018). As for the other four terms, the product of horizontal internal tidal velocity and horizontal shear of horizontal near-inertial velocity ($u_T\partial u_f/\partial x$ and $v_T\partial u_f/\partial y$; Fig. 7a and b) is a little larger than $w_f\partial u_T/\partial z$, which is one order of magnitude smaller than $w_T\partial u_f/\partial z$; whereas the product of horizontal near-inertial velocity and horizontal shear of horizontal internal tidal velocity ($u_f\partial u_T/\partial x$ and $v_f\partial u_T/\partial y$; Fig. 7d and e) is approximately 1/6 to 1/3 of $w_T\partial u_f/\partial z$ on the average. Based on these results, we can conclude that in the deep ocean near the LS, the interaction between the M_2 ITs and NIWs is also dominated by the product of vertical internal tidal velocity and vertical shear of horizontal near-inertial velocity, which is followed by the product of horizontal near-inertial velocity and horizontal shear of horizontal internal tidal velocity, whereas the other terms can be neglected.

4.4. Influence of IT-NIW interaction on the evolution of NIKE

According to Equation (6), the interaction between the M_2 ITs and NIWs can modulate the energy exchange between ITs and NIWs [–

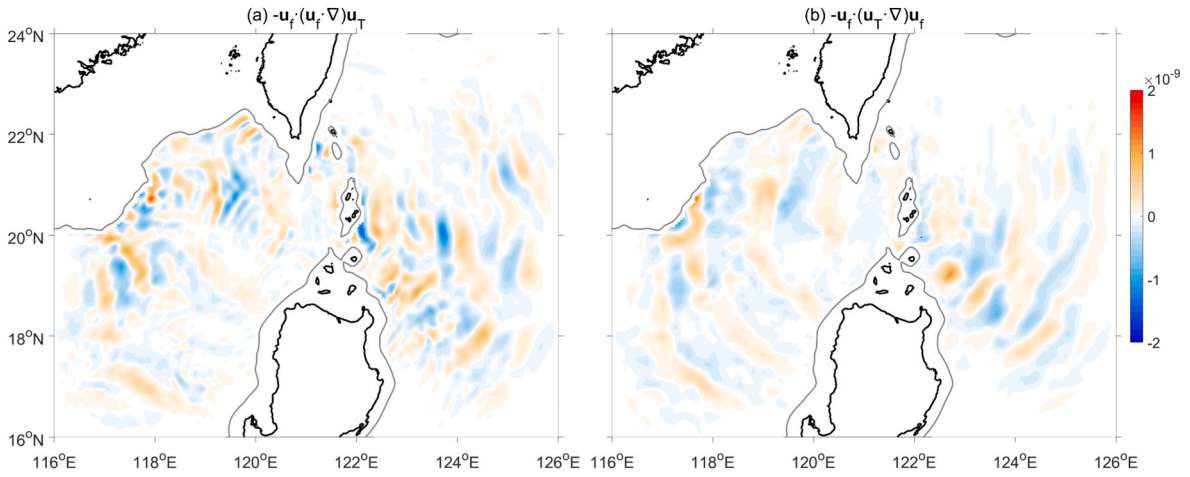

Fig. 8. Time-averaged values (shading, unit: m^2/s^3) of (a) $-\mathbf{u}_f\cdot(\mathbf{u}_f\cdot\nabla)\mathbf{u}_T$, (b) $-\mathbf{u}_f\cdot(\mathbf{u}_T\cdot\nabla)\mathbf{u}_f$ and (c) their sum averaged in the upper 1000 m. The gray curve denotes the 1000 m isobath.

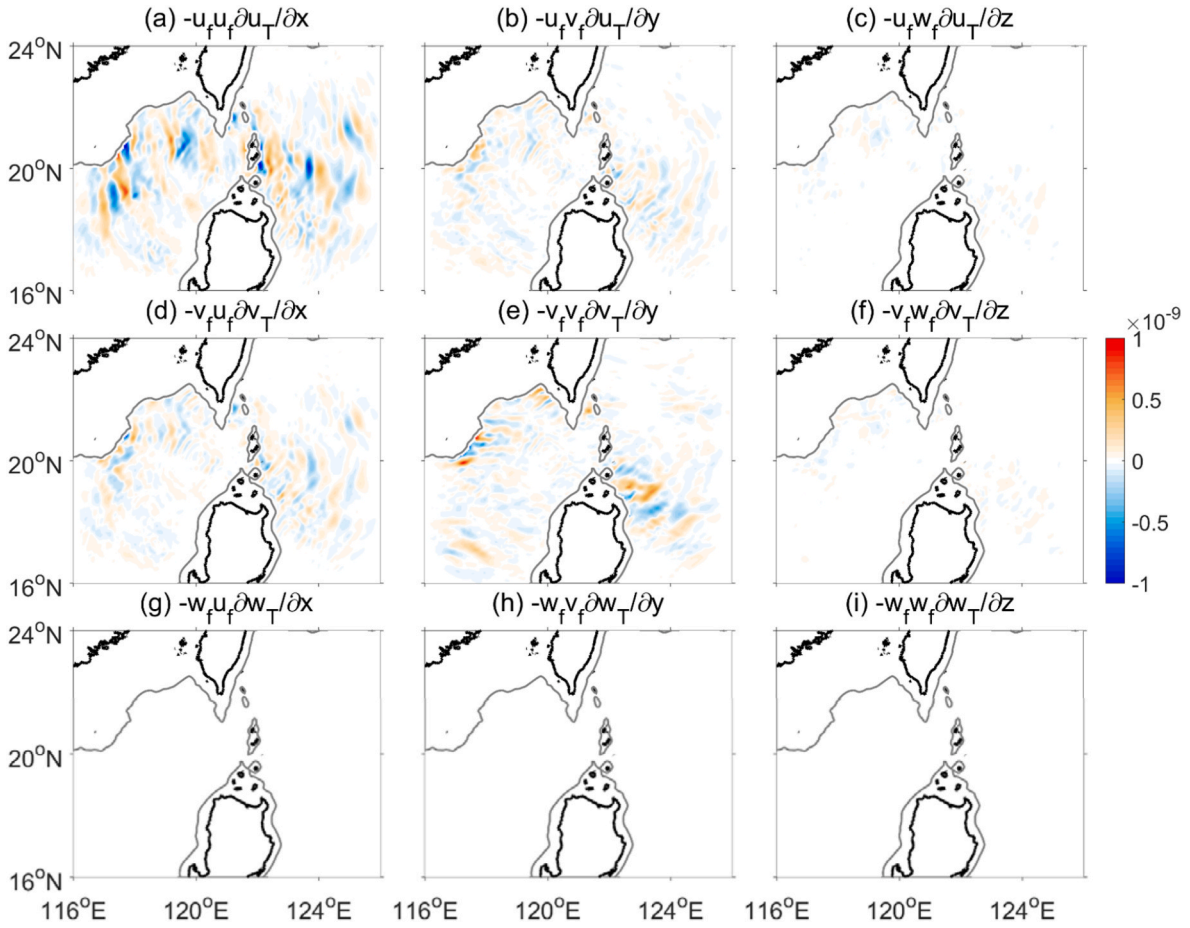

Fig. 9. Time-averaged value (shading, unit: m^2/s^3) of each term in $-\mathbf{u}_f\cdot(\mathbf{u}_f\cdot\nabla)\mathbf{u}_T$ averaged in the upper 1000 m. The gray curve denotes the 1000 m isobath.

$\mathbf{u}_f\cdot(\mathbf{u}_f\cdot\nabla)\mathbf{u}_T$] and near-inertial energy flux [$-\mathbf{u}_f\cdot(\mathbf{u}_T\cdot\nabla)\mathbf{u}_f$], which finally influence the evolution of NIKE. To understand these influences, Fig. 8 displays the time-depth-averaged values of $-\mathbf{u}_f\cdot(\mathbf{u}_f\cdot\nabla)\mathbf{u}_T$ and $-\mathbf{u}_f\cdot(\mathbf{u}_T\cdot\nabla)\mathbf{u}_f$. In terms of intensity, $-\mathbf{u}_f\cdot(\mathbf{u}_f\cdot\nabla)\mathbf{u}_T$ and $-\mathbf{u}_f\cdot(\mathbf{u}_T\cdot\nabla)\mathbf{u}_f$ are comparable, suggesting that their influences on the evolution of NIKE are similarly significant. The signs of $-\mathbf{u}_f\cdot(\mathbf{u}_f\cdot\nabla)\mathbf{u}_T$ and $-\mathbf{u}_f\cdot(\mathbf{u}_T\cdot\nabla)\mathbf{u}_f$ indicate that the interaction between the M_2 ITs and NIWs on the evolution of NIKE can either enhance or reduce their magnitude. This influence is site-dependent. Moreover, $-\mathbf{u}_f\cdot(\mathbf{u}_f\cdot\nabla)\mathbf{u}_T$ has more small-scale variations than $-\mathbf{u}_f\cdot(\mathbf{u}_T\cdot\nabla)\mathbf{u}_f$.

Figs. 9 and 10 further display the contribution of each term to $-\mathbf{u}_f\cdot(\mathbf{u}_f\cdot\nabla)\mathbf{u}_T$ and $-\mathbf{u}_f\cdot(\mathbf{u}_T\cdot\nabla)\mathbf{u}_f$, respectively. It is interesting to find that the ITs and NIWs have different influences on $-\mathbf{u}_f\cdot(\mathbf{u}_f\cdot\nabla)\mathbf{u}_T$ and $-\mathbf{u}_f\cdot(\mathbf{u}_T\cdot\nabla)\mathbf{u}_f$. In the modulation of energy exchange between ITs and NIWs [$-\mathbf{u}_f\cdot(\mathbf{u}_f\cdot\nabla)\mathbf{u}_T$], the terms associated with horizontal shear of horizontal internal tidal velocity (Fig. 9a, b, 9d and 9e) play crucial roles

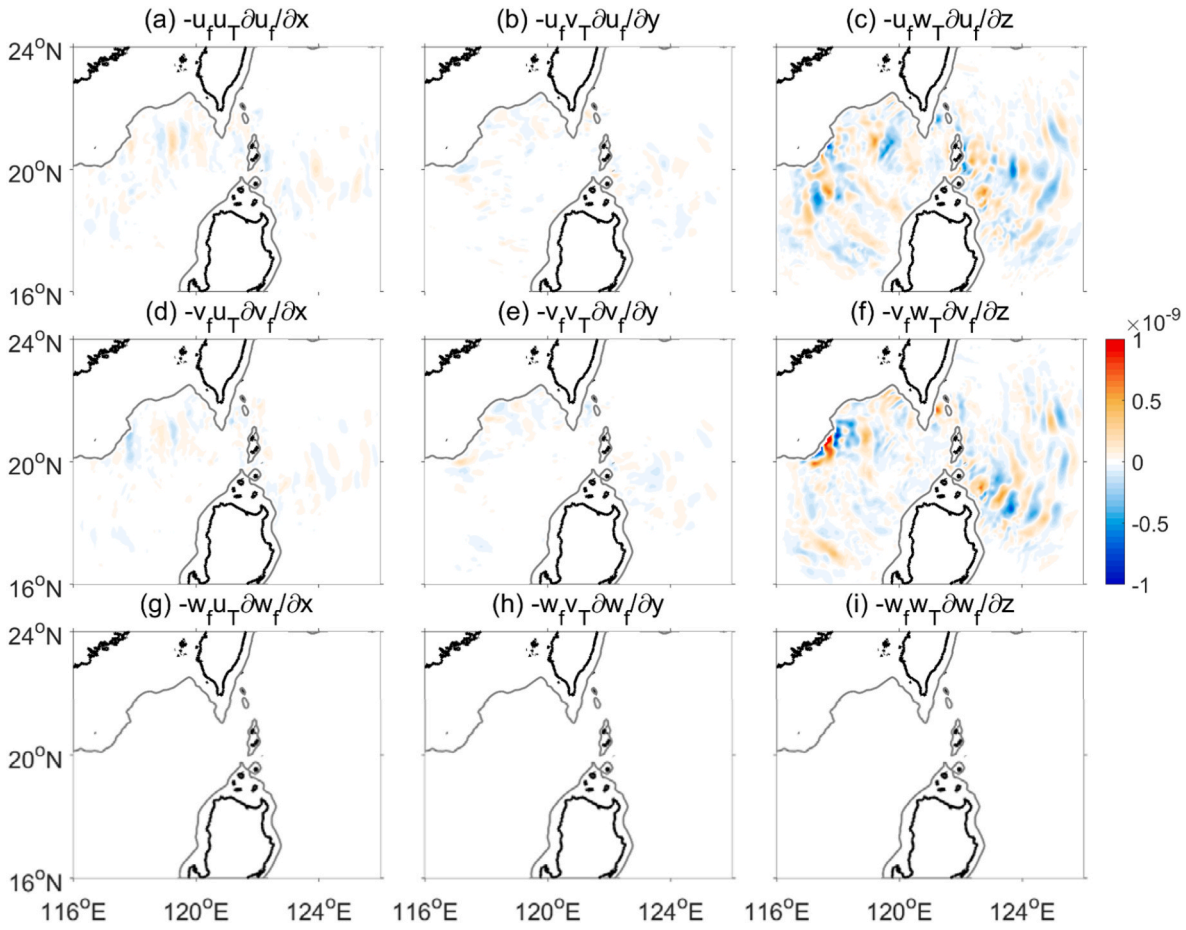

Fig. 10. Same as Fig. 9 but for $-\mathbf{u}_f\cdot(\mathbf{u}_T\cdot\nabla)\mathbf{u}_f$.

and other terms are too small to be noticed. In contrast, the terms associated with vertical shear of horizontal near-inertial velocity (Fig. 10c and f) are dominant in the modulation of near-inertial energy flux and other terms can be neglected. We believe that these results deepen our understanding of the evolution of NIKE under the IT-NIW interaction.

5. Discussions and conclusions

In this study, we explore the interaction between the M_2 ITs and typhoon Megi-induced NIWs in the deep ocean near the LS based on the numerical simulation results. Results of this study highlight the importance of the M_2-*f* waves to the shear enhancement. Although the KE of the M_2-*f* waves is one order of magnitude smaller than that of the M_2 ITs, the domain-averaged vertical shear squared caused by the M_2-*f* waves is comparable to that of the M_2 ITs. The reason is that the M_2-*f* waves have a large proportion of high modes whereas the M_2 ITs are dominated by low modes (Figs. 5 and 6), which have been demonstrated by in situ observations (Cao et al., 2018). The M_2-*f* waves also cause intense shear in another IT-NIW interaction, i.e. resonant triad interaction (Nikurashin and Legg, 2011; Liang and Wunsch, 2015; Wang et al., 2021). Note that the IT-NIW interaction investigated in this study and resonant triad interaction are different: In the former, both the ITs and NIWs are parent waves and the *f*M_2 and M_2-*f* waves are child waves (Section 2); whereas in the latter, only the ITs are the parent wave and the M_2-*f* waves and NIWs are child waves (Nikurashin and Legg, 2011; Liang and Wunsch, 2015; Wang et al., 2021). Given that both the IT-NIW interaction investigated in this study and resonant triad interaction are ubiquitous in the ocean, the internal waves with the frequency equal to the difference of those of ITs and NIWs should be taken into consideration for the improvement of parameterizations of turbulent mixing driven by internal waves.

The contribution of each term to the IT-NIW interaction in the deep ocean near the LS is evaluated. Results indicate that the product of vertical internal tidal velocity and vertical shear of horizontal near-inertial velocity dominates over the other terms, and the product of vertical near-inertial velocity and vertical shear of horizontal internal tidal velocity is the weakest. This result is consistent with observations in the shallow water in the SCS (Guan et al., 2014; Lin et al., 2015; Liu et al., 2018). As for the products of horizontal internal tidal (near-inertial) velocity and horizontal shear of horizontal near-inertial (internal tidal) velocity, which cannot be evaluated by observations from one single mooring, they are not negligibly weak. Actually, the product of horizontal near-inertial velocity and horizontal shear of horizontal internal tidal velocity can reach 1/6 to 1/3 of the product of vertical internal tidal velocity and vertical shear of horizontal near-inertial velocity, which makes a considerable contribution to the IT-NIW interaction.

The IT-NIW interaction also affects the evolution of NIKE by modulating the energy exchange and near-inertial energy flux. However, the modulations of energy exchange and near-inertial energy flux are contingent upon the specific site characteristics. Moreover, the ITs and NIWs are found to have different influences on the modulations of energy exchange and near-inertial energy flux. In the modulation of energy exchange, the terms associated with horizontal shear of horizontal internal tidal velocity are dominant. Whereas in the modulation of near-inertial energy flux, the terms associated with vertical shear of horizontal near-inertial velocity are important.

CRediT authorship contribution statement

Anzhou Cao: Writing – review & editing, Writing – original draft, Visualization, Methodology, Funding acquisition, Conceptualization. **Zheng Guo:** Writing – review & editing, Writing – original draft, Methodology, Funding acquisition. **Xu Chen:** Writing – review & editing, Supervision. **Xinyu Guo:** Writing – review & editing, Supervision. **Jinbao Song:** Writing – review & editing, Supervision.

Data availability

The data used in this study are available in the Zenodo at https://doi.org/10.5281/zenodo.14327083.

Declaration of competing interest

The authors declare that they have no known competing financial interests or personal relationships that could have appeared to influence the work reported in this paper.

Acknowledgements

This study is supported by the National Natural Science Foundation of China (Grant Number: 42176002). This study is partly supported by the Ministry of Education, Culture, Sports, Science and Technology, Japan (MEXT) to a project on Joint Usage/Research Center–Leading Academia in Marine and Environment Pollution Research (LaMer). Anzhou Cao acknowledges the Funding of ZJU Tang Scholar. The authors also thank Dr. Shuya Wang for constructive discussions as well as the editor and reviewers for valuable comments.

Data availability

Data will be made available on request.

References

Alford, M.H., 2020. Global calculations of local and remote near-inertial-wave dissipation. J. Phys. Oceanogr. 50, 3157–3164. https://doi.org/10.1175/JPO-D-20-0106.1.

Alford, M.H., Mackinnon, J.A., Nash, J.D., et al., 2011. Energy flux and dissipation in Luzon Strait: two tales of two ridges. J. Phys. Oceanogr. 41, 2211–2222. https://doi.org/10.1175/JPO-D-11-073.1.

Alford, M.H., MacKinnon, J.A., Simmons, H.L., Nash, J.D., 2016. Near-inertial internal gravity waves in the ocean. Annu. Rev. Mar. Sci. 8, 95–123. https://doi.org/10.1146/annurev-marine-010814-015746.

Alford, M.H., Peacock, T., Mackinnon, J.A., et al., 2015. The formation and fate of internal waves in the South China Sea. Nature 521, 65–69. https://doi.org/10.1038/nature14399.

Buijsman, M.C., Ansong, J.K., Arbic, B.K., et al., 2016. Impact of parameterized internal wave drag on the semidiurnal energy balance in a global ocean circulation model. J. Phys. Oceanogr. 46, 1399–1419. https://doi.org/10.1175/JPO-D-15-0074.1.

Cao, A., Guo, Z., Lv, X., et al., 2017. Coherent and incoherent features, seasonal behaviors and spatial variations of internal tides in the northern South China Sea. J. Mar. Syst. 172, 75–83. https://doi.org/10.1016/j.jmarsys.2017.03.005.

Cao, A., Guo, Z., Song, J., et al., 2018. Near-inertial waves and their underlying mechanisms based on the South China sea internal wave experiment (2010–2011). J. Geophys. Res.: Oceans 123, 5026–5040. https://doi.org/10.1029/2018JC013753.

Cao, A., Guo, Z., Wang, S., et al., 2019. Upper ocean shear in the northern South China Sea. J. Oceanogr. 75, 525–539. https://doi.org/10.1007/s10872-019-00520-x.

Cao, A., Guo, Z., Wang, S., et al., 2023a. Energetics of theM2 internal tides modulated by typhoons at the Luzon Strait. Ocean Model. 186, 102243. https://doi.org/10.1016/j.ocemod.2023.102243.

Cao, A., Wang, S., Morimoto, A., et al., 2023b. Modal content of typhoon-induced near-inertial waves around the East China Sea. Continent. Shelf Res. 264, 105055. https://doi.org/10.1016/j.csr.2023.105055.

Carter, G.S., Fringer, O.B., Zaron, E.D., 2012. Regional models of internal tides. Oceanography 25, 56–65. https://doi.org/10.5670/oceanog.2012.42.

Chen, G., Xue, H., Wang, D., et al., 2013. Observed near-inertial kinetic energy in the northwestern South China Sea. J. Geophys. Res.: Oceans 118, 4965–4977. https://doi.org/10.1002/jgrc.20371.

Davies, A.M., Xing, J., 2003. On the interaction between internal tides and wind-induced near-inertial currents at the shelf edge. J. Geophys. Res. 108 (C3), 3009. https://doi.org/10.1029/2002JC001375.

Egbert, G.D., Erofeeva, S.Y., 2002. Efficient inverse modeling of barotropic ocean tides. J. Atmos. Ocean. Technol. 19, 183–204. doi: 10.1175/1520-0426 (2002)019<0183: EIMOBO>2.0.CO;2.

Guan, S., Zhao, W., Huthnance, J., et al., 2014. Observed upper ocean response to typhoon Megi (2010) in the northern South China sea. J. Geophys. Res.: Oceans 119, 3134–3157. https://doi.org/10.1002/2013JC009661.

Guo, P., Fang, W., Liu, C., et al., 2012. Seasonal characteristics of internal tides on the continental shelf in the northern South China Sea. J. Geophys. Res. 117. https://doi.org/10.1029/2011JC007215.

Guo, Z., Cao, A., Lv, X., et al., 2020. Impact of multiple tidal forcing on the simulation of the M2 internal tides in the northern South China Sea. Ocean Dynam. 70, 187–198. https://doi.org/10.1007/s10236-019-01324-9.

Hazewinkel, J., Winters, K.B., 2011. PSI of the internal tide on a β plane: flux divergence and near-inertial wave propagation. J. Phys. Oceanogr. 41, 1673–1682. https://doi.org/10.1175/2011JPO4605.1.

He, H., Cao, A., Wang, Y., et al., 2022. Evolution of oceanic near-inertial waves induced by typhoon Sarika (2016) in the South China Sea. Dynam. Atmos. Oceans 100, 101332. https://doi.org/10.1016/j.dynatmoce.2022.101332.

Li, J., Zhai, X., Liu, J., et al., 2022. Spatial and seasonal variations of near-inertial kinetic energy in the upper South China Sea: Role of synoptic atmospheric systems. Prog. Oceanogr. 208, 102899. https://doi.org/10.1016/j.pocean.2022.102899.

Liang, C.-R., Chen, G.-Y., Shang, X.-D., et al., 2019. Observation of enhanced nonlinear interactions after severe tropical storm Chanchu (2004) in the western South China Sea. J. Geophys. Res.: Oceans 124, 3837–3848. https://doi.org/10.1029/2018JC014839.

Liang, X., Wunsch, C., 2015. Note on the redistribution and dissipation of tidal energy over mid-ocean ridges. Tellus 67. https://doi.org/10.3402/tellusa.v67.27385.

Lin, F., Liang, C., Hou, Y., et al., 2015. Observation of interactions between internal tides and near-inertial waves after typhoon passage in the northern South China Sea. Chin. J. Oceanol. Limnol. 33, 1279–1285. https://doi.org/10.1007/s00343-015-4253-0.

Lin, F., Zhu, L., Zhou, B., et al., 2022. Observations of strong near-inertial currents induced by the reflection of tropical cyclone-induced near-inertial waves on the continental slope of the northern South China Sea. Deep-Sea Research Pt 190, 103893. https://doi.org/10.1016/j.dsr.2022.103893.

Liu, J., He, Y., Li, J., et al., 2018. Cases study of nonlinear interaction between near-inertial waves induced by typhoon and diurnal tides near the Xisha Islands. J. Geophys. Res.: Oceans 123, 2768–2784. https://doi.org/10.1029/2017JC013555.

Miao, C., Chen, H., Lü, X., 2011. An isopycnic-coordinate internal tide model and its application to the South China Sea. Chin. J. Oceanol. Limnol. 29, 1339–1356. https://doi.org/10.1007/s00343-011-1023-5.

Munk, W., Wunsch, C., 1998. Abyssal recipes II: Energetics of tidal and wind mixing. Deep-Sea Research Pt 45, 1977–2010. https://doi.org/10.1016/S0967-0637(98)00070-3.

Müller, M., 2013. On the space-and time-dependence of barotropic-to-baroclinic tidal energy conversion. Ocean Model. 72, 242–252. https://doi.org/10.1016/j.ocemod.2013.09.007.

Nikurashin, M., Legg, S., 2011. A mechanism for local dissipation of internal tides generated at rough topography. J. Phys. Oceanogr. 41, 378–395. https://doi.org/10.1175/2010JPO4522.1.

Niwa, Y., Hibiya, T., 2011. Estimation of baroclinic tide energy available for deep ocean mixing based on three-dimensional global numerical simulations. J. Oceanogr. 67, 493–502. https://doi.org/10.1007/s10872-011-0052-1.

Niwa, Y., Hibiya, T., 2014. Generation of baroclinic tide energy in a global three dimensional numerical model with different spatial grid resolutions. Ocean Model. 80, 59–73. https://doi.org/10.1016/j.ocemod.2014.05.003.

Onuki, Y., Hibiya, T., 2015. Excitation mechanism of near-inertial waves in baroclinic tidal flow caused by parametric subharmonic instability. Ocean Dynam. 65, 107–113. https://doi.org/10.1007/s10236-014-0789-3.

Qiao, M., Cao, A., Song, J., et al., 2022. Enhanced turbulent mixing in the upper ocean induced by super typhoon Goni (2015). Rem. Sens. 14, 2300. https://doi.org/10.3390/rs14102300.

Simmons, H.L., Hallberg, R.W., Arbic, B.K., 2004. Internal wave generation in a global baroclinic tide model. Deep-Sea Research Pt II 51, 3043–3068. https://doi.org/10.1016/j.dsr2.2004.09.015.

St Laurent, L.C., Simmons, H.L., Jayne, S.R., 2002. Estimating tidally driven mixing in the deep ocean. Geophys. Res. Lett. 29, 2106. https://doi.org/10.1029/2002GL015633.

Wang, S., Cao, A., Chen, X., et al., 2021. On the resonant triad interaction over mid-ocean ridges. Ocean Model. 158, 101734. https://doi.org/10.1016/j.ocemod.2020.101734.

Wang, G., Su, J., Ding, Y., Chen, D., 2007. Tropical cyclone genesis over the South China Sea. J. Mar. Syst. 68 (3–4), 318–326. https://doi.org/10.1016/j.jmarsys.2006.12.002.

Xing, J., Davies, A.M., 2002. Processes influencing the nonlinear interaction between inertial oscillations, near inertial internal waves and internal tides. Geophys. Res. Lett. 29 (5), 1067. https://doi.org/10.1029/2001GL014199.

Yang, B., Hou, Y., Hu, P., et al., 2015. Shallow ocean response to tropical cyclones observed on the continental shelf of the northwestern South China Sea. J. Geophys. Res.: Oceans 120, 3817–3836. https://doi.org/10.1002/2015JC010783.

Yang, Q., Zhao, W., Liang, X., et al., 2016. Three-dimensional distribution of turbulent mixing in the South China Sea. J. Phys. Oceanogr. 46, 769–788. https://doi.org/10.1175/JPO-D-14-0220.1.

Zhao, Z., 2014. Internal tide radiation from the Luzon Strait. J. Geophys. Res.: Oceans 119. https://doi.org/10.1002/2014JC010014.
Zhao, Z., 2019. Mapping internal tides from satellite altimetry without blind directions. J. Geophys. Res.: Oceans 124. https://doi.org/10.1029/2019JC015507.
Zhao, Z., Alford, M.H., MacKinnon, J.A., et al., 2010. Long-range propagation of the semidiurnal internal tide from the Hawaiian Ridge. J. Phys. Oceanogr. 40, 713–736. https://doi.org/10.1175/2009JPO4207.1.